

PUSAT PENGURUSAN PENYELIDIKAN (RMC)

BORANG PENGESAHAN LAPORAN AKHIR PENYELIDIKAN

TAJUK PROJEK : HYDROXYAPATITE COATING WITH OXIDE INTERLAYER ON
BIOMEDICAL GRADE COBALT BASED ALLOY

Saya : MAS AYU BT HASSAN (B.Eng, M.Eng, Ph.D)

(HURUF BESAR)

Mengaku membenarkan **Laporan Akhir Penyelidikan** ini disimpan di Perpustakaan Universiti Malaysia Pahang dengan syarat-syarat kegunaan seperti berikut :

1. Laporan Akhir Penyelidikan ini adalah hakmilik Universiti Malaysia Pahang
2. Perpustakaan Universiti Malaysia Pahang dibenarkan membuat salinan untuk tujuan rujukan sahaja.
3. Perpustakaan dibenarkan membuat penjualan salinan Laporan Akhir Penyelidikan ini bagi kategori TIDAK TERHAD.
4. * Sila tandakan (/)

SULIT

(Mengandungi maklumat yang berdarjah keselamatan atau Kepentingan Malaysia seperti yang termaktub di dalam AKTA RAHSIA RASMI 1972).

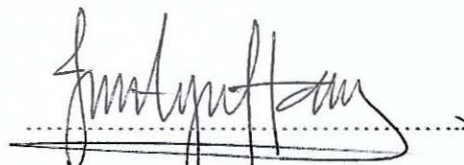
TERHAD

(Mengandungi maklumat TERHAD yang telah ditentukan oleh Organisasi/badan di mana penyelidikan dijalankan).

TIDAK
TERHAD

Tandatangan & Cop Ketua Penyelidik

DR MAS AYU BINTI HASSAN
PENSYARAH KANAN
FAKULTI KEJURUTERAAN MEKANIKA
UNIVERSITI MALAYSIA PAHANG
26600 PEKAN, PAHANG
TEL: 09-424 6316 FAX: 09-424 6222



Tarikh : 7/6/2017

CATATAN : *Jika Laporan Akhir Penyelidikan ini SULIT atau TERHAD, sila lampirkan surat daripada pihak berkuasa/organisasi berkenaan dengan menyatakan sekali sebab dan tempoh laporan ini perlu dikelaskan sebagai SULIT dan TERHAD.

**HYDROXYAPATITE COATING WITH OXIDE INTERLAYER ON
BIOMEDICAL GRADE COBALT BASED ALLOY**



MAS AYU BINTI HASSAN

(B.Eng, M.Eng, Ph.D)

**RESEARCH VOTE NO:
RDU 1403118**

**Fakulti Kejuruteraan Mekanikal
Universiti Malaysia Pahang**

2017

ACKNOWLEDGEMENT

“In the name of Allah the most gracious and the most merciful”

Alhamdulillah, I praise to Allah for His help and guidance that I am able to undergo and complete the project research successfully.

In addition, I would like to thank to all RDU1403118 team members who have helped me a lot during this project processes. Thanks for the commitment and all the cooperation given in order to finish this project.

My deepest appreciation also goes to all students under my supervision and lab assistants in Faculty of Mechanical Engineering, Universiti Malaysia Pahang.

Special thanks to all technicians of Biomedical Engineering Lab and Tissue Culture Lab, Universiti Teknologi Malaysia for helping and providing me slot within their busy schedule.

Last but not least, thank you very much to Department of Research and Innovation, Universiti Malaysia Pahang for funding this research work.



UMP

ABSTRACT

Surface modification is often required in order to improve the biological and tribological properties of metallic implants. In this research, Co-Cr-Mo alloy was oxidized in atmospheric condition to create oxide interlayer (Cr_2O_3) at different temperatures (850°C, 1050°C and 1250°C) for 3 hours prior to hydroxyapatite (HA) coating. The effect of oxide interlayer on the adhesion strength of HA coating on oxidized Co-Cr-Mo substrate was investigated. The surface of oxide interlayer was rough and contained abundant of pores, which helps in providing better mechanical interlocking to HA coating. Scanning electron microscopy and X-ray diffraction techniques were used to characterize the surface morphology of the HA coating whilst a Revetest scratch test was used to measure the adhesion strength of HA coating on oxidized substrates. The oxide interlayer on the substrate was able to prevent severe cracks while maintaining the porosity of the coated layer. Scratch test results showed that adhesion strength of the HA coating on substrates with interlayer was significantly higher than those without interlayer (1.40 N Vs 1.04 N; $p < 0.05$). These findings suggest that the porous oxide interlayer provides better anchorage whilst minimizing surface cracks of HA on Co-Cr-Mo substrates. Biocompatibility test on the HA coated substrates with oxide interlayer also demonstrate strong attachment and proliferation of cells than the HA coated substrates without oxide interlayer. It is concluded that the introduction of intermediate oxide layer on Co-Cr-Mo substrate prior to HA coating has shown a positive effect in terms of increment of the adhesion strength of HA coating as well as cell bioactivity performance.

ABSTRAK

Modifikasi permukaan sentiasa diperlukan untuk meningkatkan sifat biologi dan tribologi sesuatu implant logam. Dalam kajian ini, Kobalt-Kromium-Molibdenum (Co-Cr-Mo) aloi telah dioksidakan dalam keadaan atmosfera untuk mewujudkan lapisan teroksida (Kromium Oksida, Cr_2O_3) pada suhu yang berbeza (850°C , 1050°C dan 1250°C) untuk 3 jam sebelum salutan hidroksiapatit (HA). Kesan lapisan oksida terhadap kekuatan lekatan HA pada substrat teroksida Co-Cr-Mo telah dijalankan. Permukaan lapisan oksida didapati kasar dan mengandungi banyak liang kecil, yang membantu menyediakan pautan mekanikal yang lebih baik bagi salutan HA. Teknik pengimbasan elektron mikroskop dan pembelauan X-ray digunakan untuk mencirikan morfologi permukaan salutan HA manakala ujian calar Revetest pula digunakan untuk mengukur kekuatan lekatan salutan HA pada substrat teroksida. Didapati lapisan oksida di atas substrat dapat menghalang rekahan yang teruk sekaligus mengekalkan keliangan pada lapisan yang disalut. Ujian calar menunjukkan kekuatan lekatan salutan HA di atas substrat dengan lapisan oksida lebih tinggi berbanding salutan HA di atas substrat tanpa lapisan oksida (1.40N Vs 1.04N ; $p < 0.05$). Penemuan ini mencadangkan bahawa keliangan lapisan oksida dapat menyediakan pautan yang lebih baik sekaligus meminimumkan rekahan permukaan pada HA di atas substrat Co-Cr-Mo. Ujian bioaktiviti yang dijalankan ke atas salutan HA dengan lapisan oksida juga menunjukkan lekatan yang kuat serta percambahan sel berbanding salutan HA tanpa lapisan oksida. Kesimpulannya, pembentukan pengantara lapisan oksida di atas Co-Cr-Mo sebelum salutan HA menunjukkan kesan positif dari segi peningkatan kekuatan salutan HA dan juga prestasi bioaktiviti sel.

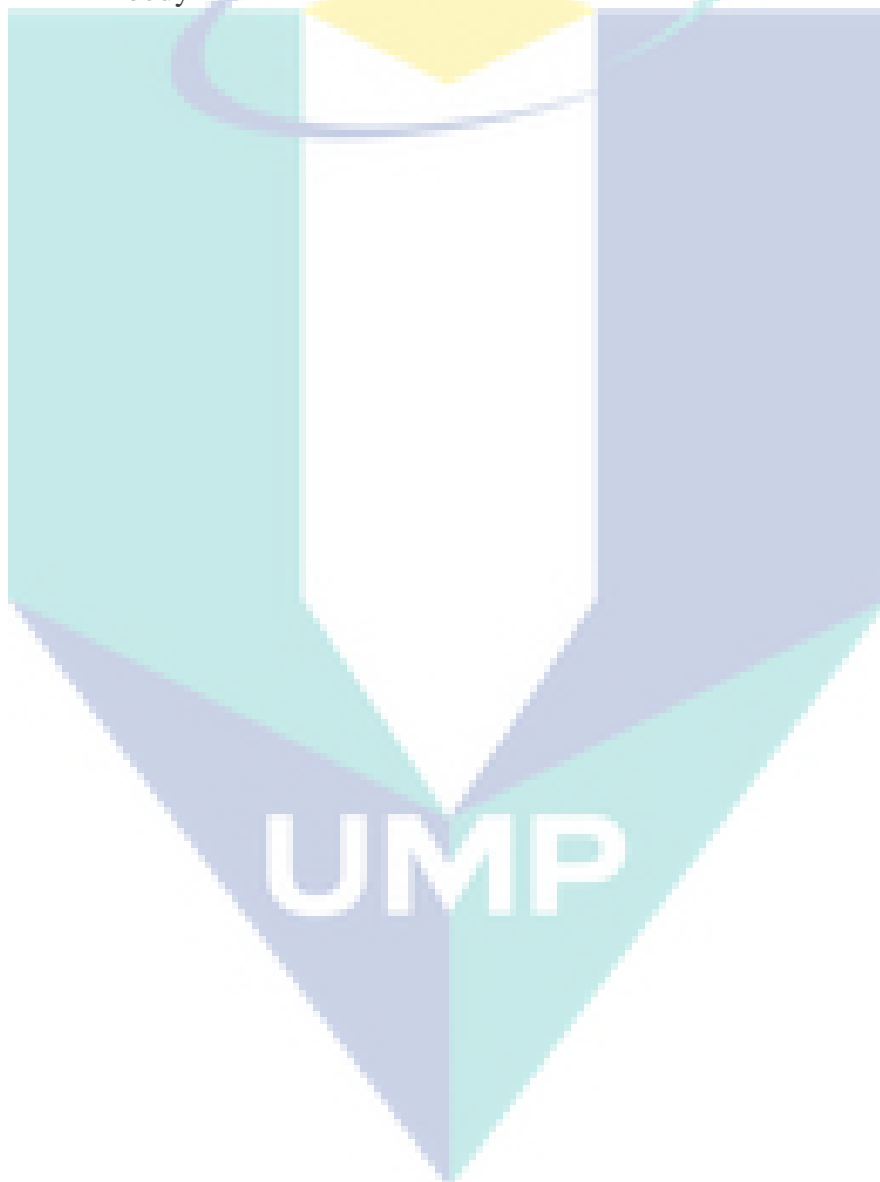
TABLE OF CONTENTS

CHAPTER	TITLE	PAGE
	ACKNOWLEDGEMENT	ii
	ABSTRACT	iii
	ABSTRAK	iv
	TABLE OF CONTENTS	v
	LIST OF TABLES	vii
	LIST OF FIGURES	viii
	LIST OF APPENDICES	x
1	INTRODUCTION	1
	1.1 Research Background	1
	1.2 Problem Statement	1
	1.3 Objectives of the Research	2
	1.4 Scopes of the Research	2
	1.5 Project Flow Chart	3
2	LITERATURE REVIEW	4
	2.1 Co-Cr-Mo Alloy as Biomaterial Implant	4
	2.2 Current Issues with Co-Cr-Mo Alloy Implants	5
	2.3 Methods for Coating HA on Co-Cr-Mo Alloy	7
3	METHODOLOGY	10
	3.1 Experimental Material and Sample Preparation	10
	3.1.1 Surface Grinding of the Samples	10

3.2	Thermal Oxidation Process	11
3.3	Preparation of HA Slurry, Dip Coating Process and Sintering Procedure	11
3.3.1	Preparation of HA Slurry	12
3.3.2	Procedure of Sol-gel Dip Coating Process	12
3.3.3	Procedure of Sintering Process	13
3.4	Adhesion Strength Test Procedure	13
3.5	Biocompatibility Test - Cell Attachment Study	14
3.6	Field Emission Scanning Electron Microscope (FESEM)	15
3.7	X-ray Diffraction (XRD)	15
3.8	Atomic Force Microscope (AFM)	16
4	RESULTS AND DISCUSSION	18
4.1	Introduction	18
4.2	Objective 1	18
4.2.1	Results on Thermal Oxidation Process	18
4.2.2	Surface Roughness Analysis of Oxidized Samples	22
4.2.3	Results on Oxide Interlayer Adhesion Strength	24
4.3	Objective 2	25
4.3.1	Results on HA Coating Deposition	25
4.3.2	Adhesion Strength Test on HA Coating	26
4.4	Objective 3	28
4.4.1	Bioactivity Analysis – Cell Attachment Study	28
5	CONCLUSIONS AND RECOMMENDATIONS	31
5.1	Conclusions	31
5.2	Recommendations	32
	REFERENCES	33
	Appendices A – E	37 – 41

LIST OF TABLES

TABLE NO.	TITLE	PAGE
2.1	Mechanical properties of cobalt based alloy recommended for surgical implants according to ASTM standard	5
2.2	Various conditions of implants versus the effects to human body	6



LIST OF FIGURES

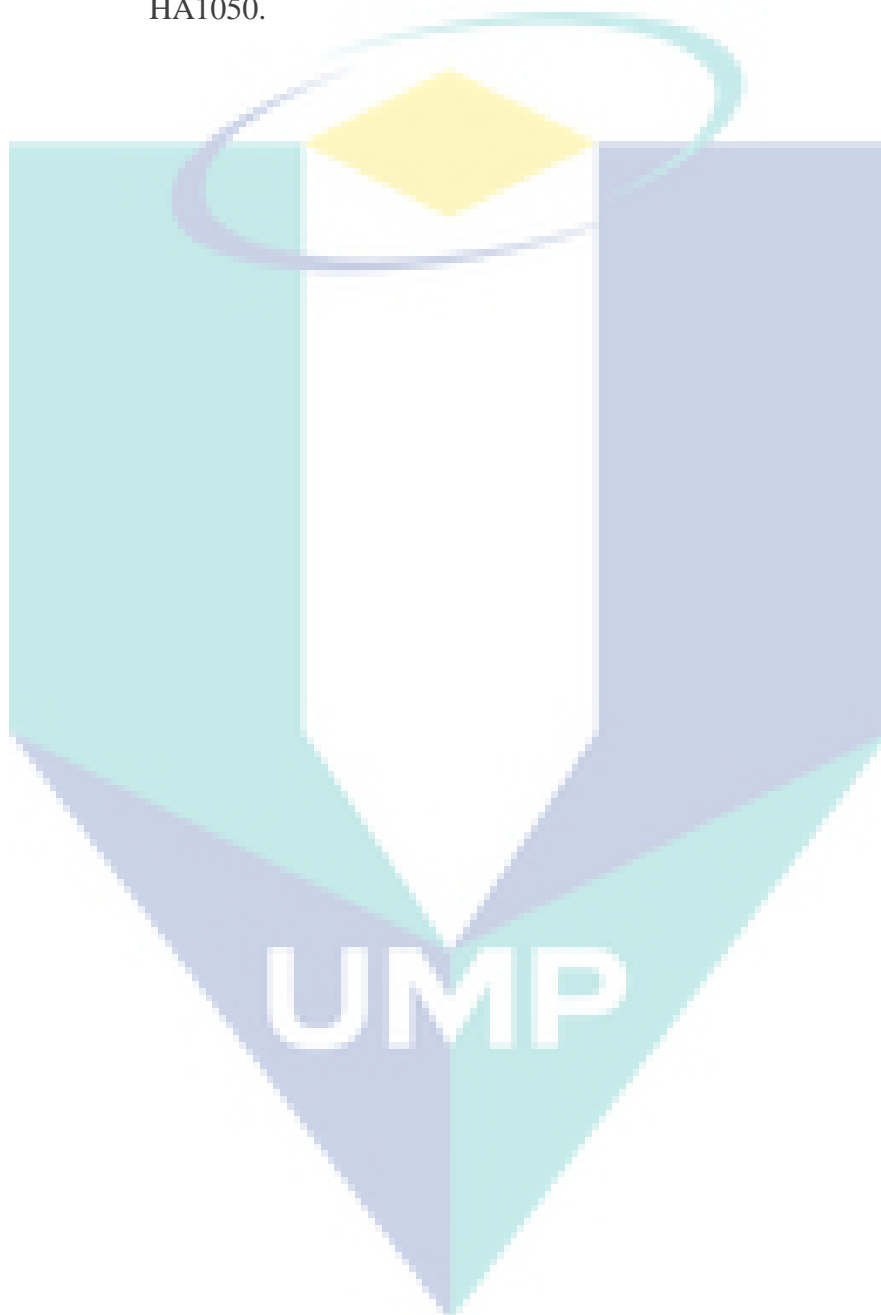
FIGURE NO.	TITLE	PAGE
1.1	The overall project flow chart.	3
3.1	(a) Dimension of cut Co-Cr-Mo alloy substrate. (b) Ground samples after undergone pickling process.	10
3.2	(a) HTWL-01 Desktop Dip Coater machine to deposit HA on the samples. (b) Closed-up view of the dip coater machine.	13
3.3	FESEM with EDX attachment used to examine the samples morphology of oxide interlayer and HA coating.	15
3.4	X-ray diffraction used to determine composition and phase analysis of the oxidized samples and HA coated samples.	16
3.5	Atomic Force Microscope used to evaluate surface roughness of oxidized samples and HA coated samples.	17
4.1	Surface morphology and cross-section of oxide interlayer formed at temperatures; (a) and (b) 850°C, (c) and (d) 1050°C, (e) and (f) 1250°C.	19
4.2	XRD patterns obtained on oxidized samples at various temperature, (a) 850°C, (b) 1050°C and (c) 1250°C, in air after 3 hours.	20
4.3	AFM micrograph of Co-Cr-Mo alloy surface roughness. (a) Before oxidation and after oxidation at temperature; (b) 850°C and (c) 1050°C, in atmosphere condition.	23
4.4	Scratch testing results showing the plots of friction coefficient, friction force and normal force. The inset shows scratching track captured from the samples treated at different conditions: (a) oxidized at 1050°C and (b) oxidized at 850°C.	24
4.5	FESEM micrographs of sintered HA coated samples at; (a) 550°C with oxide interlayer, (b) 650°C with oxide interlayer, (c) 750°C with oxide interlayer and (d) 750°C without oxide interlayer.	26
4.6	Scratch testing results showing the plots of friction	

coefficient, friction force and normal force. The inset shows scratching track captured from the samples. (a) HA1050 and (b) HA850.

27

4.7 FESEM images of MSCs on (a and b) untreated Co-Cr-Mo alloy, (c and d) HAuntreated, (e and f) HA850 and (g and h) HA1050.

30



LIST OF APPENDICES

APPENDIX	TITLE	PAGE
A	Gantt Charts and Milestone of Research Activities	37
B	ICDD database for Cr_2O_3 (No.: 38-1479)	38
C	ICDD database for $\text{Mn}_{1.5}\text{Cr}_{1.5}\text{O}_4$ (No.: 33-0892)	39
D	ICDD database for $\text{Co}_{0.8}\text{Cr}_{0.2}$ (No.: 01-071-7109)	40
E	Publications	41



UMP

CHAPTER 1

INTRODUCTION

1.1 RESEARCH BACKGROUND

Cobalt chromium molybdenum (Co-Cr-Mo) alloys have long been used for orthopaedic and dental implants due to their good mechanical and biocompatibility properties [1, 2]. To improve the implant performance, HA coatings were introduced, resulting in increased implant bioactivity and bone bonding ability [3, 4]. It has also been demonstrated that HA reduces the release of potentially harmful metal ions and protects against corrosion [5-7]. Several methods of coating HA onto these implants have been previously described. These include plasma spraying [8], sputtering process [9, 10], biomimetic [11, 12], electrochemical deposition [13, 14] and sol-gel [13, 15, 16, 17]. Among these, the use of sol-gel technique provides many advantages: high HA purity, homogeneous composition and low synthesis temperature (25°C - 800°C) [4, 18, 19]. The use of direct sol-gel HA coating onto implants has been widely reported for titanium [15, 20-22] and steel based alloys [23-26]. However, the use of sol-gel technique on Co based implants have not been reported although the use of other techniques such as investment casting [27], electrophoretic deposition (EPD) [14] and biomimetic [28] have shown to be successful.

1.2 PROBLEM STATEMENT

Despite the many advantages of HA coating, poor adhesion strength between HA and the underlying substrate [29-31] and the low cohesive strength of the coated material [31, 32] are still major issues which remain unresolved. These issues often

results in severe cracks and delamination of HA from the substrates, which would eventually lead to implant failure [29, 31-33]. To overcome these issues, researchers have designed an intermediate layer that, when placed between the brittle HA and the substrate, enhances the adhesive metal-ceramic (HA) bonding and coating integrity [24, 29]. However, many of the techniques and expertise required to produce this effect is costly and are usually technically challenging. Furthermore, the use of such techniques on Co-Cr-Mo alloys has never been established. In this research, a potential method of cheap, reliable and quick way to produce chromium oxide (Cr_2O_3) interlayer on Co-Cr-Mo substrate through an oxidation process will be introduced. Based on extensive literature studies, this is the first study ever described using sol-gel technique for coating HA on Co-Cr-Mo alloy.

1.3 OBJECTIVES OF THE RESEARCH

- i. To evaluate the surface characterization and performances of oxide interlayer introduced on the Co-Cr-Mo alloy through thermal oxidation process in terms of adhesion strength.
- ii. To evaluate the effectiveness of formed oxide interlayer in terms of HA coating adhesion on Co-Cr-Mo alloy.
- iii. To compare the performance of HA coated with oxide interlayer against HA coated without oxide interlayer in terms of cell growth and cell attachment morphologies.

1.4 SCOPES OF THE RESEARCH

The research was conducted in the following limits:

- i. Cobalt-Chromium-Molybdenum (Co-Cr-Mo) alloy was used as the substrate material.

- ii. Thermal oxidation process was used to create oxide interlayer on Co-Cr-Mo alloy within temperatures range of 850°C to 1250°C at fixed time duration in atmospheric condition.
- iii. HA coating was deposited on the samples using HTWL-01 Desktop Dip Coater (MTI Cooperation, USA) at room temperature.
- iv. The adhesion strength of oxide interlayer and HA coating were measured using Revetest Scratch test in order to determine the critical load.
- v. In-vitro biocompatibility of the HA coated samples was tested up to 14 days for cell attachment study.

1.5 PROJECT FLOWCHART

The overall project flow was described in Figure 1.1 below.

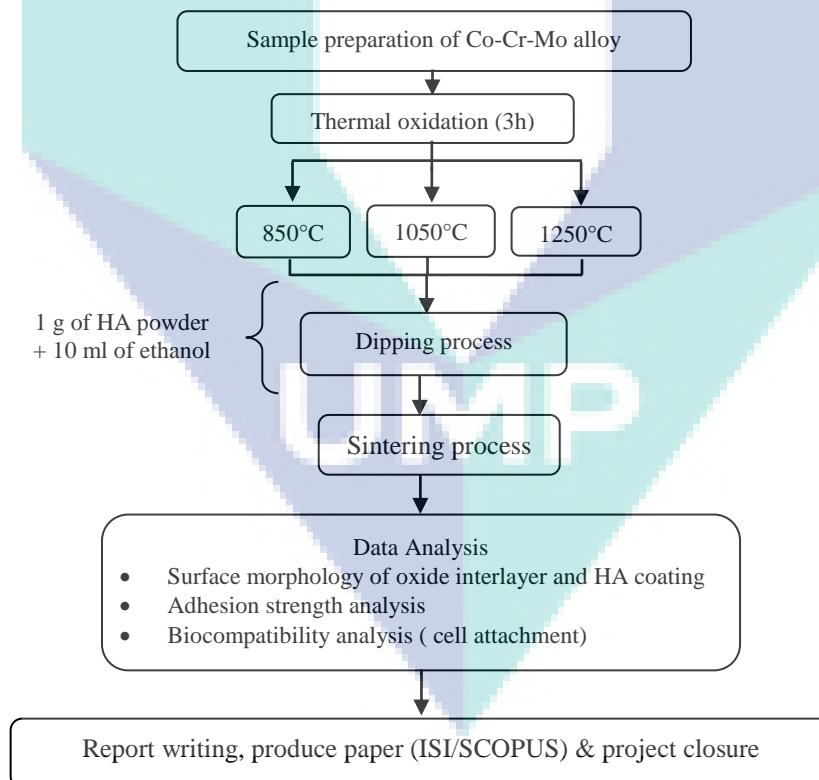


FIGURE 1.1: The overall project flow chart.

CHAPTER 2

LITERATURE REVIEW

2.1 Co-Cr-Mo Alloy as Biomaterial Implant

Cobalt based alloy or more particularly Cobalt-Chromium-Molybdenum (Co-Cr-Mo) alloy is widely used in aerospace and gas turbines technologies due to its capability of high temperature and corrosion resistance [1, 2]. Later, its applications have been extended into other areas such as biomedical implants mainly because of their good combination of mechanical properties and its high biocompatibility. Researchers have reported that Co-Cr-Mo alloy were firstly used in metal-on-metal (MOM) implants as hip and knee joints arthroplasty over 40 years ago [3]. The expanding usage of Co-Cr-Mo alloy as orthopaedic implants are expected due to their high strength with modulus of elasticity (210 – 230 GPa), excellent fatigue resistance and corrosion resistance compared to 316L stainless steel [4-6]. The presence of chromium (Cr) imparts the corrosion resistance and the small addition amounts of other elements such as tungsten, iron and molybdenum can give excellent abrasion resistance and high temperature properties [7, 8]. Furthermore, the presence of thin passive oxide film (nanometer thick) predominantly chromium oxide (Cr_2O_3) which forms spontaneously on the alloy surface have contributes an excellent corrosion resistance that closely related in enhancing its biocompatibility [9-11]. Table 2.1 presents the details of mechanical properties for various types of biomedical grade cobalt based alloy.

Table 2.1 Mechanical properties of cobalt based alloy recommended for surgical implants according to ASTM standard.

Property	Cast CoCrMo	Wrought CoCrWNi	Wrought CoNiCrMo (F562)	
	(F75)	(F90)	Solution Annealed	Cold-Worked and Aged
Tensile strength (MPa)	655	860	793–1000	1793 min.
Yield strength (0.2% offset) (MPa)	450	310	240–655	1585
Elongation (%)	8	10	50.0	8.0
Reduction of area (%)	8	—	65.0	35.0
Fatigue strength (MPa) ^a	310	—	—	—

Although there has been a long clinical experience with the usage of Co-Cr-Mo alloy as bioimplants, closer inspections revealed that the theoretical disadvantage of dissemination of metal particles and ions releases throughout the human body is a natural cause of anxiety [12]. Based on the literature surveys, several problems have arisen with the used of Co-Cr-Mo alloy as metallic implants and still remain unsolved such as implant corrosion, wear and fretting effect (degradation and cracks at surface implant) [13] which may leads to tribocorrosion (material degradation process due to the combined effect of corrosion and wear) [14, 15] and the release of metal ions that induce inflammation and allergen [16]. Moreover, recent clinical reports have claimed that bare material of Co-Cr-Mo alloy after implantation also has difficulties to bond or connect with the hard tissues that may cause to impair organs and implant failure to the patient [17, 18]. These immune reactions frequently caused the requirement for a second surgery to remove damage implants. This situation not only increasing the risks of infection, but it also increases the medical cost for both parties such as the patient and the healthcare system.

2.2 Current Issues with Co-Cr-Mo Alloy Implants

Metallic alloy that are used for implant applications should be able to provide appropriate mechanical support, biocompatible, exhibit favourable surface properties such as promoting adhesion and provide an environment where cells can maintain their

physical and biochemical characteristics (phenotypes). Table 2.2 provides the various conditions of implant and their effects to human tissues after the post-operation.

Table 2.2 Various conditions of implant versus the effects to human body [14, 19].

Condition of implant	Effect
Toxic	The surrounding bone tissue dies
Nontoxic and biologically inactive	A fibrous tissue of variable thickness forms
Nontoxic and biologically active (bioactive)	An interfacial bond forms (implants with the hard tissues)
Nontoxic and dissolves	An interfacial bond forms

Co-Cr-Mo alloy have long being used as prosthetic implant in orthopedic surgery especially for load bearing biomedical applications owing to their excellent corrosion resistance, wear resistance, and mechanical properties. [17]. However, due to its metallic nature, Co-Cr-Mo alloy exhibits slow osteointegration which typically takes duration from 3 to 6 months and lack of bioactivity limit. It also has proven that this metallic materials is difficult to connect or bond directly to host tissues after implantation owing to encapsulation by fibrous tissues [10, 17, 20, 21]. Consequently, inadequate compatibility of the implant surface with the bone tissues also can result in fixation failures and undesired inflammatory responses which later leads to necessitate for revision surgery [22]. Due to these reasons, Co-Cr-Mo alloy often requires surface treatment before it can be applied as orthopaedic implants.

In order to improve the implant-tissues osseointegration, continuous efforts have been devoted into modifying the Co-Cr-Mo alloy surface [17, 23, 24]. Many potential bioceramics coating materials such as alumina, zirconia, tricalcium phosphate and hydroxyapatite have been investigated based on their ability to induce bone regeneration and bone growth at the implant-tissue interface without the intermediate fibrous tissue layer [8, 25]. Among the various types of bioceramics material, hydroxyapatite, HA ($\text{Ca}_{10}(\text{PO}_4)_3(\text{OH})_2$) has received the most attention for coating on load bearing implant applications due to bone tissue has been found to have the ability to form a bond with HA. [8, 26]. There are several deposition techniques that have been used to coat HA on

the metallic implants such as thermal spray, physical deposition method and biomimetic processes [25]. However, one of the critical parts in producing bioceramic coatings is to develop a stable and good adhesion at the coating and implant interface in order to achieve long-term success of orthopaedic and dental implants especially in Co-Cr-Mo material alloy.

Recently, there has been increasing interest in coating Co-Cr-Mo alloy with bioceramics, calcium phosphate materials such as hydroxyapatite (HA) [17, 22, 27]. Many reports revealed that by coating Co-Cr-Mo alloy with HA films, the biocompatibility of this alloy can be improved because the HA coatings promotes bone ingrowth to the implant as well as faster bone remodeling due to enhanced bi-directional growth and formation of a bonding interlayer at the implants interface [22, 28, 29]. Surface modification on metal implants especially on Co-Cr-Mo alloy have shown positive effect on osteointegration and therefore should be considered seriously for improving further their performance.

Despite the different methodologies used to deposit HA coatings, the published studies demonstrate that lack of information on the in-vitro test of Co-Cr-Mo alloy. Furthermore, it is impossible to compare the results of in-vitro experiments that have been conducted using different surface treatments and HA preparations. Therefore, more research on cell behaviour and reactions are required to understand the biological effects due to it may vary depending on surface parameters, such as the surface topography, surface chemistry and crystallinity of HA [25]. Through in-vitro test, the production of surfaces will allow researchers to understand, modulate and elicit the desired reactions from the hard tissues surrounding the implants and will ultimately lead to more satisfactory tissues regeneration.

2.3 Methods for Coating HA on Co-Cr-Mo Alloy

Recently, an extensive research on HA coating not only concentrated on the tissue-implant interface, but also focused further on other problems associated with the coating process and optimization of coating parameters in order to improve tissues

response and bone growth. The critical quality specifications for HA coatings include thickness, phase composition, crystallinity, Ca/P ratio, microstructure, surface roughness, porosity, implant type and surface texture, which influence the resulting mechanical properties of the implant, such as cohesive and bond strength, tensile strength, shear strength, Young's modulus, residual stress and fatigue life [30-32]. Changes to these variables can produce coatings with varied bioactivity and durability. It has been suggested that a coating for orthopaedic implants should have low porosity, strong cohesive strength, good adhesion to the substrate, a high degree of crystallinity and high chemical and phase stability [25].

In the past few decades, a variety of process methodologies to deposit HA on metallic Co-Cr-Mo alloy implant surfaces namely via physical methods such as plasma spraying, sputter coating and electro-deposition, meanwhile via chemical methods such as sol-gel dip coating and biomimetic processes have been employed. Most of these techniques are targeted to enhance the long-term performance of implants by encouraging bone ingrowth and providing better fixation of the implants. Moreover, coating with HA on Co-Cr-Mo alloy also has been proven to promote appropriate surface chemistry for tissues compatibility without altering the bulk mechanical properties of the material. Chemical methods are sometimes more preferred than physical methods since it is believed to be more suitable in depositing on complex and intricate surface structures of implant devices with porous morphology with intricate structures. Chemical methods also allow the liquid medium to have full access into the outer and inner surfaces at a low temperature without modifying the mechanical properties of metallic biomaterial alloy during the coating process.

Biomimetic technique is one of the chemical treatments that have widely been investigated due to its advantages to the metal implant surface [24, 33, 34]. In the case of metallic substrates, reports showed promising results on titanium alloy but not to Co-Cr-Mo alloy which probably due to the different surface characteristics of these materials. The bonelike apatite layer formed on the surface of Co-Cr-Mo alloy was claimed to be much thinner and less adherent than observed on the surface of titanium alloy [35]. Beside this technique, plasma spray deposition is another method that has been recognized as widely commercially used in the manufacturing of implants. Even

though this technique is widely used in coating orthopaedics and dental implants, but the process has been reported causing several draw backs such as poor adherence of the coating, low fracture toughness of the HA coating and lack of uniformity of the coating [8]. The higher coating thickness ($>100\ \mu\text{m}$) obtained from this technique may lead to a major problem as it can cause failure due to fatigue under tensile loading conditions. Furthermore, cracking at the coatings surface was also observed due to residual stress within the thicker coating layer [36].

Another technique that has lately received the most attention because of its well-known inherent advantages is the sol-gel dip coating method. The sol-gel dip coating method is a relatively simple way to coat HA coatings on the metallic biomaterial because of its ability to produce crystalline films at a relatively low temperature, possibility to tailor microstructures and its convenience for complex shape coatings [37]. Although the sol-gel dip coating process did not bring any significant change to the HA coating film, but the deposited film on the implant surface demonstrated the effectiveness in enhancing osteoconductivity after implantation [8, 38]. In its simplest manifestation, sol-gel method works based on the withdrawal of a sample from a colloid solution, gravitational draining and solvent evaporation accompanied by further condensation reactions and result in the deposition of thin films on the sample [25, 39, 40].



UMP

CHAPTER 3

METHODOLOGY

3.1 Experimental Material and Sample Preparation

Cobalt-Chromium-Molybdenum alloy (Co-Cr-Mo) bar was supplied with the following chemical compositions (in wt.%): C: 0.24; Cr: 29.6; Mo: 6.5; Si: 0.7; Ni: 0.1; Fe: 0.12; Mn: 0.7. N: 0.16 and Co: balance. The supplied material is according to ASTM F1537. The received bar was cut using a precision cutter (Buehler, Isomet 4000) into disc size of 14 mm diameter and 2 mm thick. The final disc shape and size are shown in Figures 3.1 (a) and (b). All discs were then drilled a through hole with diameter of 0.2 mm for holding purposes during sol-gel dip coating process.

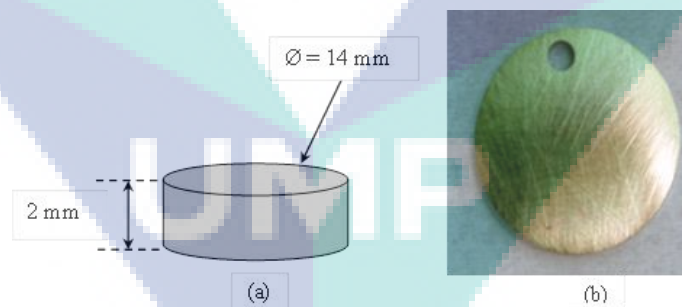


Figure 3.1 (a) Dimension of cut Co-Cr-Mo alloy substrate. (b) Ground sample surface after undergone pickling process.

3.1.1 Surface Grinding of the Samples

Grinding process is the final step for the sample preparations prior to thermal oxidation process. Grinding process was carried out in order to achieve uniform surface

roughness. All samples were ground using Struers Tegramin-25 programmable automatic sample preparation machine. They were wet ground using #500 grit SiC paper for 3 min. Both surfaces were ground in order to provide initial average of surface roughness, $R_a = 0.1 \pm 0.02 \mu\text{m}$. The purpose is to make sure that small variation in surface roughness between samples will not significantly influence the adhesion strength of the oxide interlayer formed after thermal oxidation process.

3.2 Thermal Oxidation Process

In this study, the range of thermal oxidation was carried out at 850°C, 1050°C and 1250°C, which is slightly below and above the annealing temperature (1121°C) of Co-Cr-Mo alloy. The thermal oxidation process was performed in a muffle furnace for 3 hours under atmospheric condition and left to cool inside the furnace. The heating/cooling rate was set constant at approximately 10°C/min. The oxide interlayer formed was then characterized and evaluated of its chemical composition by using Field Emission Scanning Electron Microscope (FESEM) and X-ray diffraction (XRD) respectively. Surface roughness measurement on the oxidized surface was carried out using surface profilometer (Mitutoyo SJ-301) and Atomic Force Microscope (AFM) to observe the changes in surface roughness after samples undergone thermal oxidation process. Based on the results obtained, the oxidation temperature with good surface morphology of oxide interlayer in terms of no cracks, no spallation or delamination will be selected for the further analysis.

3.3 Preparation of HA Slurry, Dip Coating Process and Sintering Procedure

Description of each process for preparation of HA slurry, dip coating process and sintering procedure is discussed in details as included in the Section 3.3.1, 3.3.2 and 3.3.3 respectively.

3.3.1 Preparation of HA Slurry

Hydroxyapatite (HA) powder ($\text{Ca}_{10}(\text{PO}_4)_6(\text{OH})_2$) used in this study was purchased from Sigma Aldrich, UK. Then, the HA powder was sieved to $\leq 71 \mu\text{m}$ particle size using RX-B6-1 Seive Shaker. This is to ensure no agglomeration of HA powder during mixture process with the ethanol. The sieved powder was kept in the desiccator to control the humidity of HA when it is not in used. HA powder was prepared by weighing for 1g, 2g and 3g using digital electronic balance SASTEC. The weighted HA powder was put separately in three different glass bottles before they were mixed with 10 ml of ethanol (CH_5OH). Prior to that, a magnetic bar was inserted in each glass bottle for stirring purposes. All bottle caps were tightly secured with parafilm to avoid any evaporation of the ethanol solution during the stirring process. In order to produce homogenously dispersed HA powder, the mixture was magnetic stirred at the speed of 600 rpm for 24 hours at room temperature. The prepared HA slurry was ready for dip coating process as described in the Section 3.4.2.

3.3.2 Procedure of Sol-gel Dip Coating Process

The HA coating deposition process was carried out using HTWL-01 Desktop Dip Coater (MT1 Cooperation, USA) at room temperature. The oxidized and untreated samples were dipped in the prepared HA slurry at fixed dipping and withdrawal speeds of 200 mm/min. Then, all HA coated samples were dried at room temperature for 3 min before being dipped again in the slurry. The dipping process was repeated for 5 times to obtain the desired HA coating thickness. Figure 3.2 shows the dip coater machine used for depositing HA on the samples.

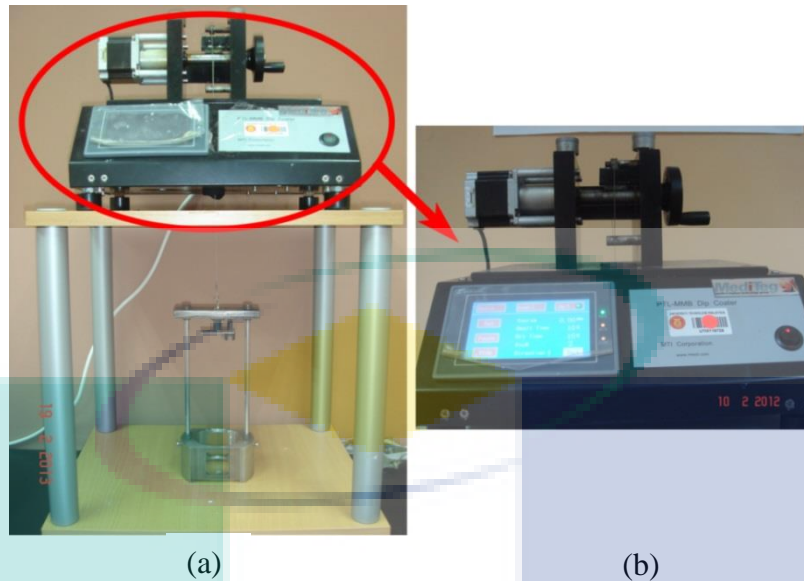


Figure 3.2 (a) HTWL-01 Desktop Dip Coater machine to deposit HA on the samples. (b) Closed-up view of the dip coater machine.

3.3.3 Procedure of Sintering Process

All HA coated samples were sintered in the muffle furnace at three different temperature range of 550°C, 650°C and 750°C for 1 hour under atmospheric condition. The heating/cooling rate was set constant at approximately 10°C/min. The samples were left to cool inside the muffle furnace before they were taken out for morphology observations and selected further experiments. Only one temperature will be chosen for details experiment based on crack free HA coating surface after sintering process.

3.4 Adhesion Strength Test Procedure

Revetest scratch test was used to determine the adhesion strength of the oxide interlayer and HA coated layers formed on the samples. A sphere-conical diamond stylus having a radius of 200 μm and angle of 120° was used to scratch the layers. Two set of scratching parameters were applied to measure the adhesion strength of oxide interlayer on the samples and the adhesion strength of HA coated samples. The reason of applying two different set of parameters was due to HA coating have weaker and

brittle structure compared to oxide interlayer. Therefore, an appropriate parameters should be applied on the HA coating in order to obtain reliable and accepted measuring results. First scratch parameters with constant load rate of 30 N/min were conducted on the oxidized samples. Oxidized samples were displaced at a constant speed of 1.36 mm/min with maximum scratched coating length of 2 mm. Second scratch parameters, is applied on HA coated samples with constant load rate at 1 N/min and the samples were moved at a constant speed of 1 mm/min with the same scratch length. The critical load of HA coating and oxide interlayer were measured for 3 times on each sample at three different locations and was determined based on the friction coefficient obtained from the friction force graphs. Scanning electron microscope (SEM, JOEL JSM-6390 LV) was used to capture the image of the scratches in order to confirm the length at which the failure was recorded.

3.5 Biocompatibility Test - Cell Attachment Study

Cell attachment analysis was performed on untreated sample (no. of samples, n=12), HAuntreated (n=12), HA850 (n=12) and HA1050 (n=12). The analysis was done at two time interval, i.e. at day 7 and day 14. Six samples were drawn from each group of samples. For instance, at day 7 six samples from untreated samples, HAuntreated, HA850 and HA1050 were taken out from each flask to be analysed on the cell activities. Observation on the cell growth and cell attachment was done using Field Emission Scanning Electron Microscope (FESEM), Zeiss Supra 35VP. Analysis of each sample group was evaluated on 6 different samples under the same condition to minimize variance of cell morphologies. Previously, MSCs cell were seeded on the untreated samples, HAuntreated, HA850 and HA1050 for 14 days. Then, at each time point of day 7 and day 14 the samples were taken for cell observations via FESEM. However, before viewing under FESEM, all samples need to be prepared in order to fix the cell on the sample through dehydration process. The dehydration process was done as the following steps:

3.6 Field Emission Scanning Electron Microscope (FESEM)

The Zeiss Supra 35VP Field Emission Scanning Electron Microscope (FESEM) as shown in Figure 3.3 was used to determine surface morphology of the oxidized samples, coating thickness and cell morphologies. The oxide interlayer and HA coating element phase were analysed using Energy-dispersive X-ray spectroscopy (EDX, Oxford INCA X-Sight) which is attached on the same equipment. Prior to the FESEM analysis, all HA coated and cell attachment samples were sputter coated with gold to prevent electrostatic charging and to obtain clear view of the cell growth behaviour.



Figure 3.3 FESEM with EDX attachment used to examine the samples morphology of oxide interlayer and HA coating.

3.7 X-ray Diffraction (XRD)

The phase composition of the oxidized sample and HA coated sample were analysed using Bruker D-8 Advance diffractometer (Figure 3.4). The parameter of grazing XRD was operated at an angle of 3° with $\text{CuK}\alpha$ radiation $\lambda = 1.5406 \text{ \AA}$. In this study, XRD pattern was recorded continuously from 2θ range of 20° to 80° with a step size of 0.05° and a step time of 1 second. Grazing XRD method was chosen to analyse the chemical composition of oxidized sample and HA coating sample because of its

effectiveness in analysis thin layer coating. In order to obtain a complete analysis of scan peak, each sample was scanned about 30 minutes.



Figure 3.4 X-ray diffractometer used to determine composition and phase analysis of the oxidized samples and HA coated samples.

3.8 Atomic Force Microscope (AFM)

The surface topography and surface roughness, Ra of oxidized and HA coated samples were characterized using a non-contact measurement i.e.; Atomic Force Microscope (AFM, SP A300 HV) as shown in Figure 3.5. The measurement size on the surface sample was $20\ \mu\text{m} \times 20\ \mu\text{m}$. AFM machine was used to analyse the surface roughness of HA coated samples because of brittleness nature of the HA coating and easily to peel-off if using direct contact method. Each sample was measured three times at different spots before an average surface roughness was determined. The results on surface topography and surface roughness of all samples were presented in graphical forms.

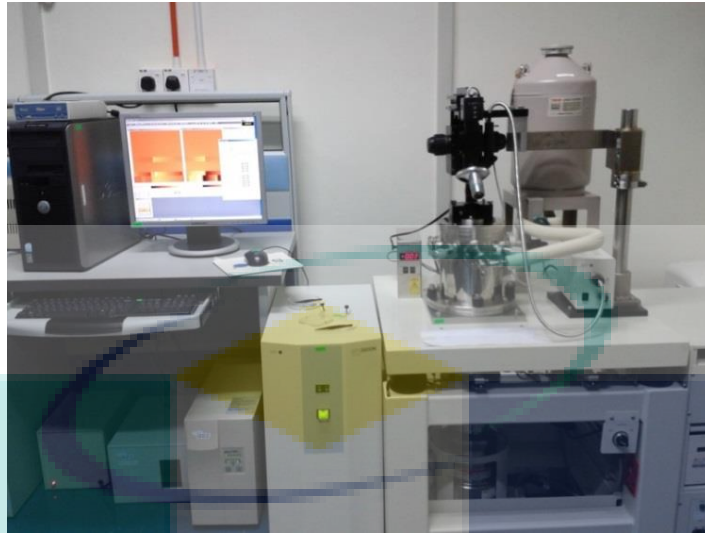


Figure 3.5 Atomic Force Microscope used to evaluate surface roughness of oxidized samples and HA coated samples.

UMP

CHAPTER 4

RESULTS AND DISCUSSION

4.1 INTRODUCTION

In this chapter, the result for all tests was studied. Results are divided into three main parts to reflect three objectives of this study respectively. The first part is consists of experimental findings for oxidized Co-Cr-Mo substrates. The second part of this chapter consists of analysis and evaluation of Co-Cr-Mo substrates after coated with HA. While, the last part consists of biocompatibility test on HA coated samples with and without oxide interlayer.

4.2 OBJECTIVES 1: To evaluate the surface characterization and performances of oxide interlayer introduced on the Co-Cr-Mo alloy through thermal oxidation process in terms of adhesion strength.

4.2.1 Results on Thermal Oxidation Process

Oxidation temperature ranges from 850°C to 1250°C was tested on Co-Cr-Mo alloy for 3 hours in order to create oxide interlayer. The experiments were performed in the atmospheric condition using muffle furnace. Analysis on the oxide interlayer such as surface morphology and cross-section images were assessed using FESEM.

After undergone thermal oxidation process, FESEM, EDX and XRD analysis were carried out on the oxidized samples to exam their surface characterization and chemical composition. Figure 4.1 shows the surface morphology (on the left) and cross-

section images of oxide interlayer (on the right) produced through thermal oxidation process at various temperatures. Figure 4.1 (a) and (b) show the oxide interlayer formed at temperature 850°C. The surface morphology of oxide interlayer exhibits no appearance of micro-cracks or spallation on the oxidized sample surface. The inset image in Figure 4.1 (a) shows the oxide interlayer appears like spikes with compact structure. As shown in Figure 4.1 (b), the oxide interlayer formed seems uniform with thickness of $1.327 \pm 0.2 \mu\text{m}$ and it also contains with neither pores nor micro-cracks. The cross-section view at this surface treatment clearly shows that the formation of oxide interlayer is dense and compact structure. These characteristics are probably suitable for HA coating on implant.

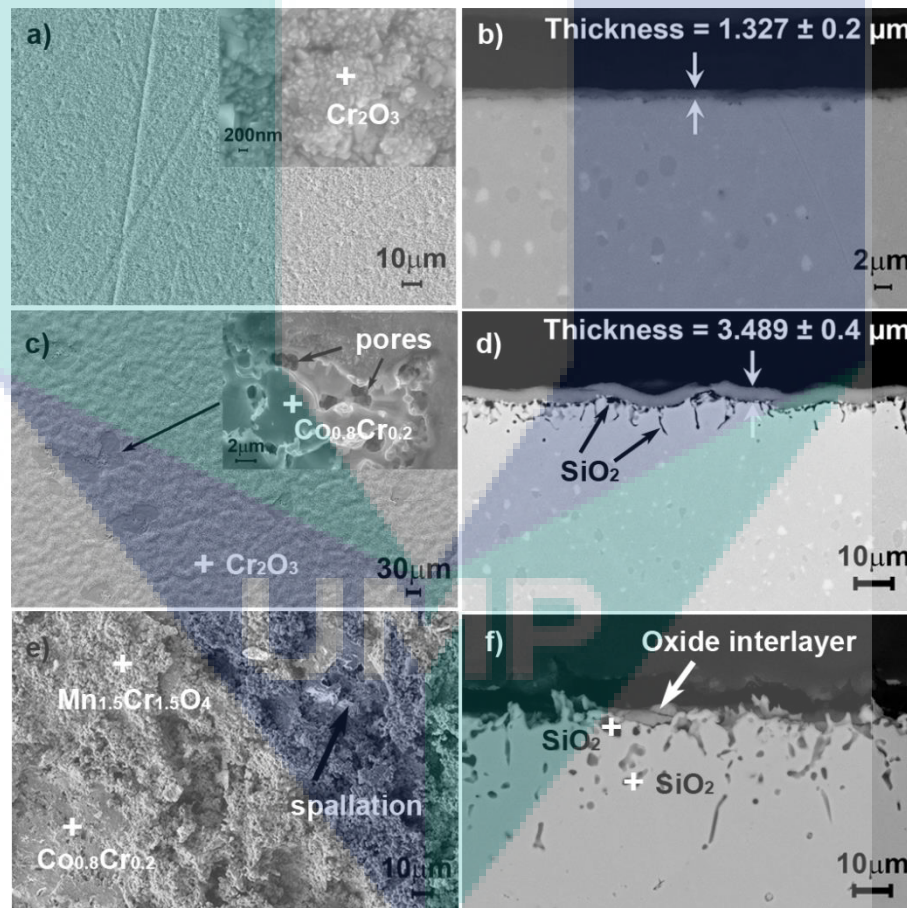


Figure 4.1 Surface morphology and cross-section of oxide interlayer formed at temperatures; (a) and (b) 850°C, (c) and (d) 1050°C, (e) and (f) 1250°C.

According to XRD results in Figure 4.2, the highest peak is Cr_2O_3 (International Centre for Diffraction Data, ICDD No.: 38-1479) with higher intensity than other

compounds. The XRD patterns also show the presence of $Mn_{1.5}Cr_{1.5}O_4$ (ICDD No.: 33-0892) and $Co_{0.8}Cr_{0.2}$ (ICDD No.: 01-071-7109) on the sample surface which formed simultaneously on the oxide interlayer as oxidation temperature increased. All ICDD documents of each compound are presented in Appendix B to Appendix D. It is believed that even at low temperature of oxidation ($850^{\circ}C$), chromium has reacted actively with other elements too such as cobalt and manganese from the bulk substrates. It is also well known that manganese and cobalt have high activation energy compared to molybdenum [7], which makes them easier to react with chromium and oxygen to transform into other compound when they received enough energy during oxidation process.

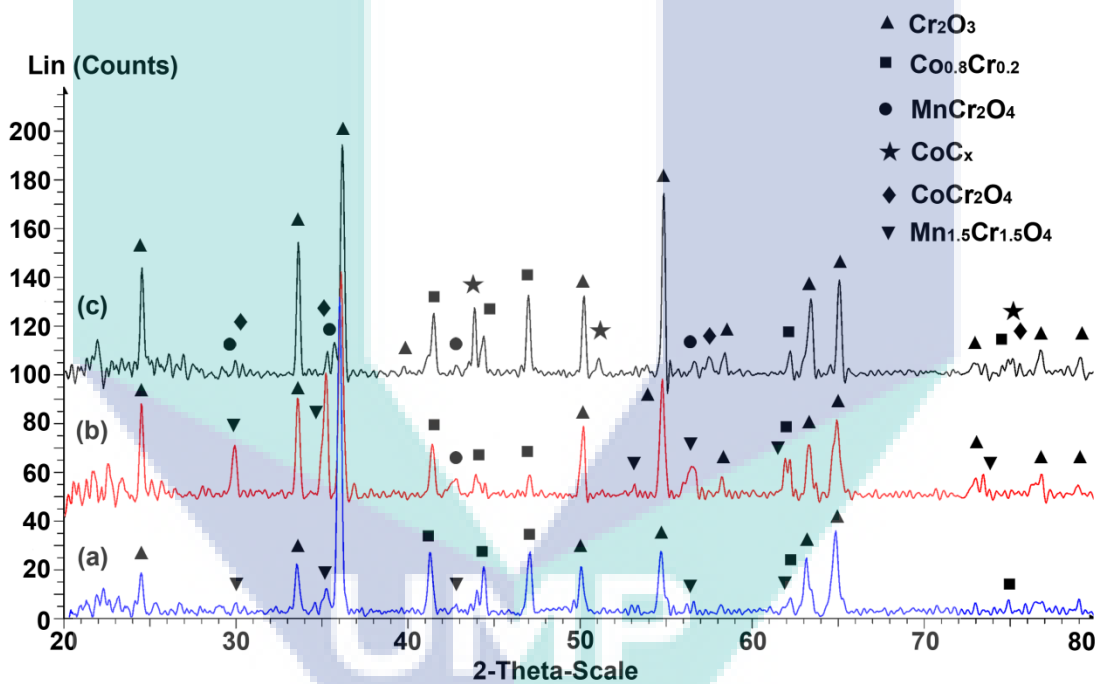


Figure 4.2 XRD patterns obtained on oxidized samples at various temperature, (a) $850^{\circ}C$, (b) $1050^{\circ}C$ and (c) $1250^{\circ}C$, in air after 3 hours.

As the oxidation temperature increased from $850^{\circ}C$ to $1050^{\circ}C$, abundant pores were scattered across the sample surface and some parts of oxide interlayer were spalled-off from the sample as shown in Figure 4.1 (c). However, it is also noticed that the majority of the oxide interlayer still remains adhered to the sample. The spallation of some parts on oxide interlayer which occurred during sample cooling from

high temperature to room temperature, probably due to the thermal expansion difference between the oxide interlayer ($7.5 \times 10^{-6}/^{\circ}\text{C}$) and the metal sample ($15 \times 10^{-6}/^{\circ}\text{C}$) [36, 39]. The EDX results has confirmed that the spalled off area on the sample surface was $\text{Co}_{0.8}\text{Cr}_{0.2}$ as shown in the inset image in Figure 4.1 (c). The cross-section image of oxidized sample at 1050°C (Figure 4.1 (d)) visibly shows the oxide interlayer looks uneven and wavy with thickness layer of $3.489 \pm 0.4 \mu\text{m}$. The thickness of oxide interlayer formed at this temperature also appeared almost 3 times thicker than oxide interlayer in 850°C sample. Based on close observation, there is some effect of internal oxidation occurred beneath the oxide interlayer which is looks like micro-cracks and scattered of black spots.

It is worth to note that the elevated oxidation temperature can caused the increment of oxide interlayer thickness. As the internal oxidation grows deeper to the bulk material at high temperature, the thicker oxide interlayer was observed. This is because of elevated temperature permits a rapid chromium supply from the bulk material substrate to form a continuous and thicker Cr_2O_3 layer when react with oxygen. Furthermore, according to thermal oxidation kinetics, higher energy also leads to form thicker oxide interlayer. This is evident by FESEM images in Figure 4.1 (b) and (d). Similar behaviour was also reported by previous researchers when they conducted thermal cyclic experiments on cobalt based alloy at much higher temperature but much longer oxidation duration [1, 2]. The oxidized sample at 1050°C might also provide better mechanical interlocking for HA coating due to porosity formed on the oxide interlayer and rougher sample surfaces obtained based on surface morphology observation in Figure 4.1 (c). Therefore, such characteristic of this oxidized sample was considered for further analysis in this study.

As the temperature was further increased up to 1250°C which is above the annealing temperature (1121°C) of Co-Cr-Mo alloy, most of the oxide interlayer were peeled-off and more severe spallation occurred on the sample surface (Figure 4.1 (e)). It is also noted that the thickness oxide interlayer was unable to be measured due to massive spallation and micro-cracks took place (Figure 4.1 (f)). Similar black spots which observed on the oxidized sample at temperature 1050°C were also seen on this sample. However, the black spots are located about $30 \mu\text{m}$ beneath the oxide interlayer.

It is believed that this phenomenon occurs due to the internal oxidation of silicon. As mentioned earlier, silicon was added in the Co-Cr-Mo alloy about 0.7 wt.% by the manufacturer to promote the reformation of a Cr_2O_3 layer during oxidation process. However, when the sample undergoes thermal oxidation at higher temperature and for a long duration, more SiO_2 precipitates in the vicinity of the alloy and at the oxide interlayer interface. Although some researchers reported that discontinuous distribution of SiO_2 is beneficial to the cyclic oxidation resistance and helps in establishing the Cr_2O_3 layer [2, 18], but in this study it caused most of the oxide interlayer peels-off from the sample. This indicates that oxidation temperature at 1250°C is not suitable for developing oxide interlayer.

When evaluating FESEM images and EDX results, oxide interlayer produced through thermal oxidation at 850°C exhibits better performance compared to the other two oxidation temperatures in terms of cracks and delamination. While, at temperature 1050°C more porosity and cracks were observed in the oxide interlayer. These surface characteristics might be an advantage for providing better anchorage of HA coating on the sample. However, thermal oxidation at 1250°C was discontinued for further investigation due to the sample experienced severe spallation of oxide interlayer and surface damages. It is believed that this condition may not be helpful in improving HA bonding or enhancing the bioactivity performances. Therefore, only 850°C and 1050°C were chosen for further investigation.

4.2.2 Surface Roughness Analysis of Oxidized Samples

Figure 4.3 illustrates surface morphologies with roughness values before and after thermal oxidation process. Atomic Force Microscope (AFM) was used to characterize the oxidized samples' surfaces. Figure 4.3 (a) shows the initial surface roughness of Co-Cr-Mo alloy before thermal oxidation. AFM expose some scratch marks on the sample surface due to grinding effect during preparing the samples. The initial surface roughness recorded before thermal oxidation is $0.14 \pm 0.02 \mu\text{m}$. It is observed that after thermal oxidation process, the surface morphology as well as surface roughness of the untreated sample Co-Cr-Mo alloy was totally modified. The oxidized

sample at 850°C (Figure 4.3 (b)) shows lower peaks and valleys of oxide structure compared to oxidized sample at 1050°C (Figure 4.3 (c)), which consists of deep curve with higher peaks and valleys. As shown in Figure 4.3, each sample condition reveals three different values of surface roughness. This figure concludes that thermal oxidation increases the surface roughness of untreated Co-Cr-Mo alloy to 2.35 times and 8.64 times when heated at 850°C and 1050°C respectively. These results are tally with FESEM images illustrated in Figure 4.1.

This phenomenon can be explained by continuous growth of epitaxial oxide layer due to elevated oxidation temperatures which subsequently, caused inhomogeneous nucleation occurred. Moreover, it is also observed that variety of compound formation at higher temperature suggesting different crystalline shape and size has grew on the sample surface. These reasons are also contribute to the increment of surface roughness in oxidized samples.

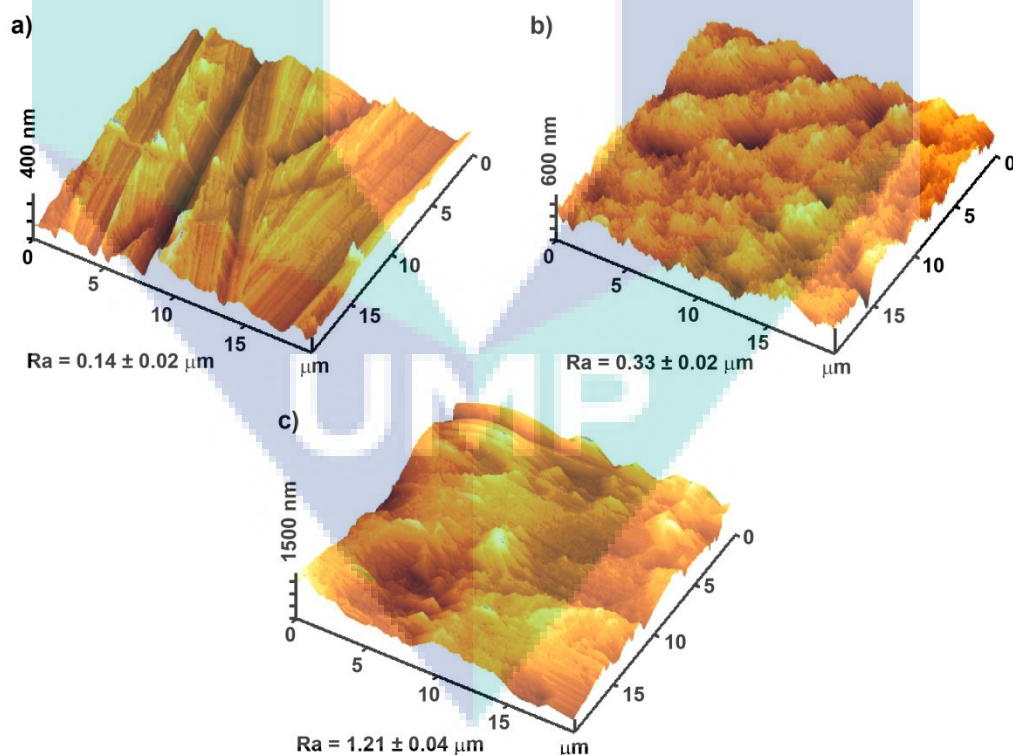


Figure 4.3 AFM micrograph of Co-Cr-Mo alloy surface roughness. (a) Before oxidation and after oxidation at temperature; (b) 850°C and (c) 1050°C, in atmosphere condition.

4.2.3 Results on Oxide Interlayer Adhesion Strength

Figures 4.4 (a) and (b) show the output graphs from the scratch tests for oxidized samples. The progressive load of 30 N/min was applied on oxidized Co-Cr-Mo substrate to measure the adhesion strength of oxide interlayer at 850°C and 1050°C. As the stylus moves forward, it scratches the oxide interlayer and simultaneously three graphs are plotted to record the changes in friction coefficient, friction force and normal load. The oxide interlayer (without HA coating) peeled-off at 6.8N and 8.63N for oxidized sample at 850°C and 1050°C respectively. The increment of critical load for oxidized sample at 1050°C was much higher than oxidized sample at 850°C. This phenomenon happened due to thicker and rougher oxide interlayer obtained in 1050°C sample as shown earlier in Figures 4.1 and 4.3.

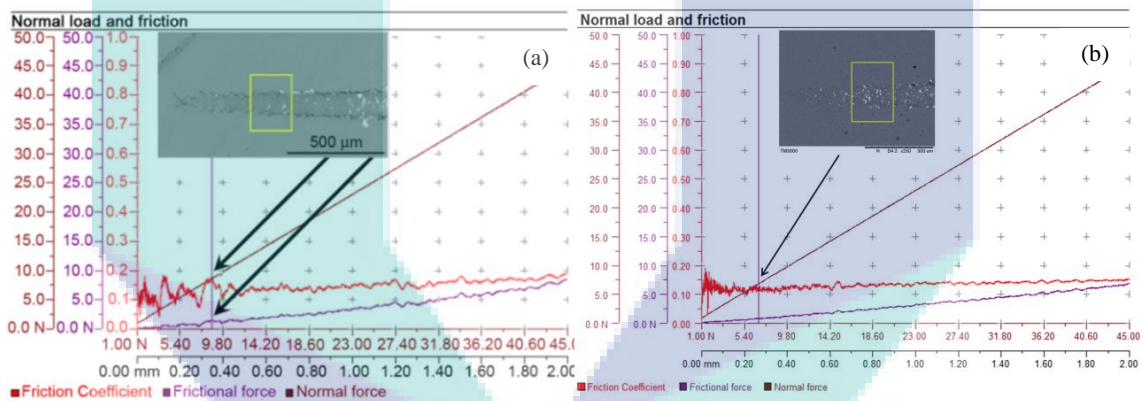


Figure 4.4 Scratch testing results showing the plots of friction coefficient, friction force and normal force. The inset shows scratching track captured from the samples treated at different conditions: (a) oxidized at 1050°C and (b) oxidized at 850°C.

4.3 OBJECTIVES 2: To evaluate the effectiveness of formed oxide interlayer in terms of HA coating adhesion on Co-Cr-Mo alloy.

4.3.1 Results on HA Coating Deposition

The HA coating on oxidized samples and untreated samples were then sintered at different sintering temperature i.e. 550°C, 650°C and 750°C for 1 hour in order to determine the optimize sintering temperature for this study.

The HA sintered surface morphologies at various temperatures with and without oxide interlayer are shown in Figure 4.5 (a) to (d). It is observed that more micro-cracks appear on HA1050 sample when sintered at the lowest temperature (550°C) and followed by HA1050 sintered at 650°C. However, there is no visible micro-crack observed on HA1050 when sintered at much higher temperature (750°C). The micro-cracks on these samples seem to be gradually reduced as the sintering temperature increases. It is believed that higher sintering temperature able to enhance the chemical bonding and the densification of HA particles with the presence of oxide interlayer.

This phenomenon may be attributed to the better gripping of HA particles on the oxidized sample at the interface. The oxidized sample at 1050°C has a rougher surface ($R_a = 1.21 \pm 0.04 \mu\text{m}$) than untreated sample ($R_a = 0.1 \pm 0.02 \mu\text{m}$). It is believed that rough surface texture plays major roles in providing better mechanical interlocking for the HA particles to hook on the sample and therefore they are not easily cracks or delaminate [18, 41, 42]. The role of oxide interlayer can be clearly seen in Figures 4.5 (c) and (d). Under the same sintering temperature of 750°C, samples without oxide interlayer show wider and deeper cracks on the HA coating surface as shown in Figure 4.5 (d). Based on the observations, sintering temperature at 750°C exhibits the best performance and therefore this temperature will be used for the whole experiments.

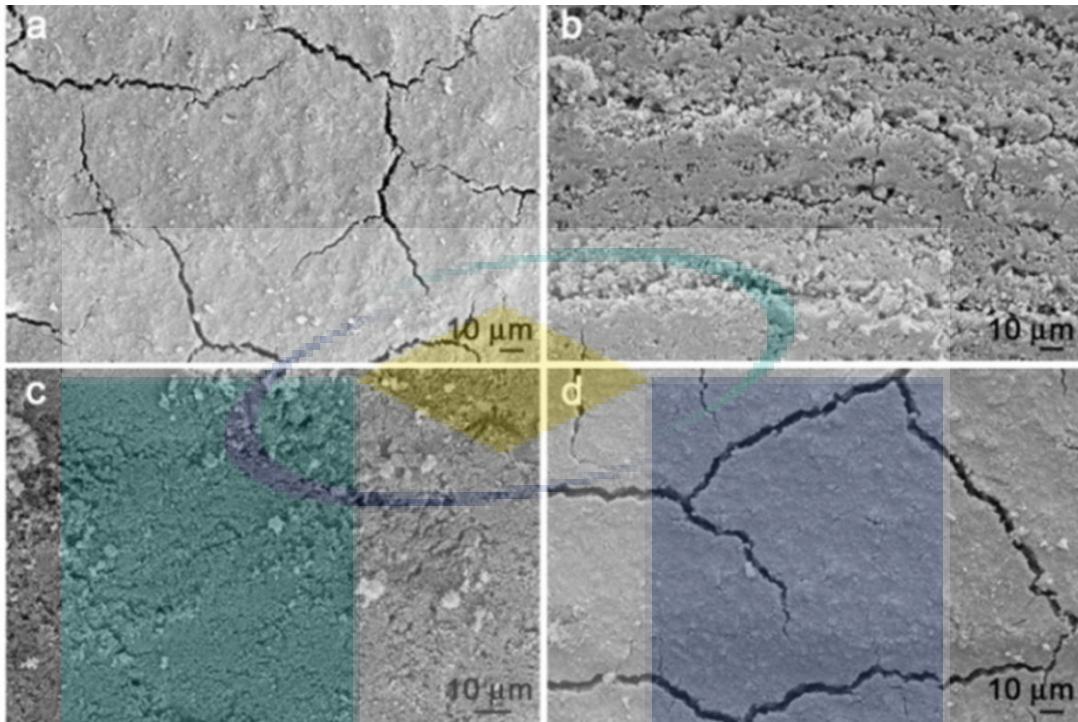


Figure 4.5 FESEM micrographs of sintered HA coated samples at; (a) 550°C with oxide interlayer, (b) 650°C with oxide interlayer, (c) 750°C with oxide interlayer and (d) 750°C without oxide interlayer.

4.3.2 Adhesion Strength Test on HA Coating

The progressive load of 1 N/min applied in the coating adhesion test was found sufficient to initiate delamination on HA coating layer deposited on the oxidized Co-Cr-Mo alloy. Revetest scratch tester is used to measure the HA coating on the HA850 sample in order to compare the critical load obtained from HA1050 sample. Figures 4.6 (a) and (b) showed the output graphs from the scratch tests carried out on HA850 sample and HA1050 sample respectively. HA coating on the oxide interlayer which oxidized at 850°C fails at the critical load of 1.25N for same sintering temperature (750°C) employed on HA1050 sample.

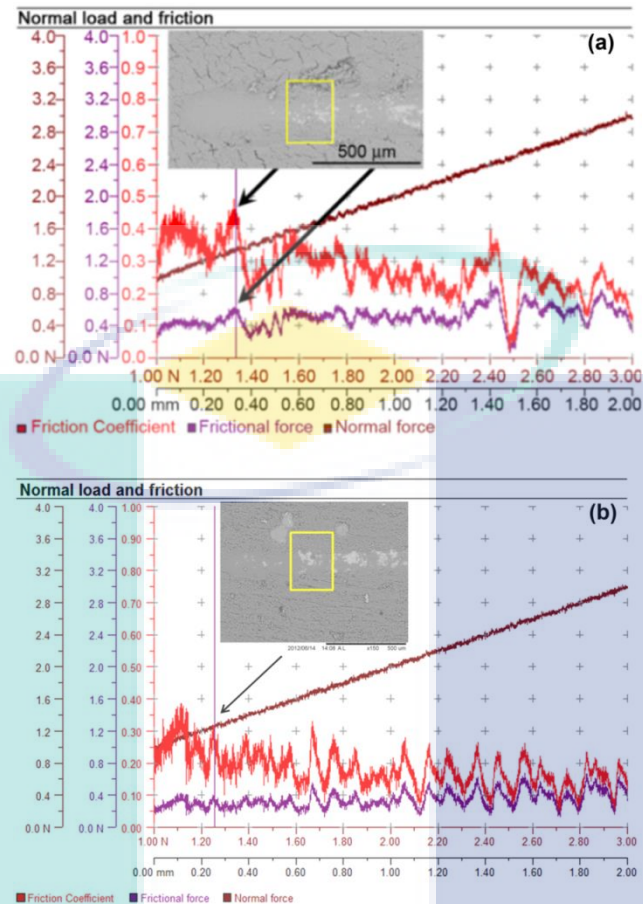


Figure 4.6 Scratch testing results showing the plots of friction coefficient, friction force and normal force. The inset shows scratching track captured from the samples. (a) HA1050 and (b) HA850.

Previously, the adhesion strength of oxide interlayer obtained at 850°C was observed to be less than oxide interlayer formed at 1050°C (6.8N vs. 8.63N) as shown in Figure 4.4. Further investigations, the adhesion strength of HA coating on oxidized 850°C also shows similar behaviour which is lower in critical load as compared to HA coating layer on oxidized 1050°C (1.25N vs. 1.40N). This phenomenon occurred due to higher oxidation temperature proportional to higher surface roughness of oxide interlayer which has provided better mechanical interlocking of HA layer on the sample surface therefore, the increment of adhesion strength in HA coating is achieved [41, 42].

Furthermore, it is also known that the roughened surface roughness is one of the factors that will increase the surface energy of the substrate material [43]. Thus in this

study, the increment of adhesion strength in HA coating-sample interface may also influence by this factor. Theoretically it can be explained by low surface energy will increased surface tension of HA intermolecular as well as impacted the HA cohesive strength. Hence, due to the high cohesive strength of HA coating in oxidized sample at 850°C, no micro-cracks were observed on the coating surface as indicated in the inset image of Figure 4.6 (b).

4.4 OBJECTIVES 3: To compare the performance of HA coated with oxide interlayer against HA coated without oxide interlayer in terms of cell growth and cell attachment morphologies.

4.4.1 Bioactivity Analysis – Cell Attachment Study

The biocompatibility of the HA coated with oxide interlayer was carried out by culturing of human osteoblast-like cells line which is known as Multipotent Stromal Cells (MSCs). The MSCs responses to the untreated sample of Co-Cr-Mo alloy and HA coated sample with and without oxide interlayer was assessed by FESEM and the resulting images are shown in Figure 4.7. The MSCs morphologies and activity were examined at time point of day 7 and day 14 on 4 different conditions of sample such as untreated sample (without HA), HAuntreated, HA850 and HA1050. Cells responses on untreated sample (Figures 4.7 (a) and (b)) were then compared with cells responses on HA coated sample with and without oxide interlayer (Figures 4.7 (c) to (h)).

Based on Figures 4.7 (a) and (b), it can be clearly seen that the MSCs cultured on untreated sample still remained in their original round shape even up to 14 days of incubation. The presence of lamellipodia shows that MSCs able to adhere on the surface of untreated sample even though at slower speed of cell growth compared to HA coated samples. This happened due to the formation of passive layer on Co-Cr-Mo alloy which eventually helps in the adhesion of MSCs. It is well known that passive layer that forms spontaneously on Co-Cr-Mo alloy surface is able to control the material's corrosion behaviour thus contributes in reducing the release of toxicity ions [44]. Similar results were also observed by other researchers when investigating cells activity on different

untreated metal samples [45]. It is also observed that the numbers of filopodium were less with small protrusion indicating slow growth of MSCs on untreated sample (Figure 4.7 (a)). After 14 days of cells cultured, the MSCs morphologies seems to experience cells damaged and cracks on its tissues surface as shown by arrows in Figure 4.7 (b). This phenomenon demonstrates poor cells' proliferation even after long period of cell culture due to low biomineralization ability of Co-Cr-Mo alloy. Further observation also revealed that propagation of filopodium is not connected with other cells probably due to stunted of cells growth.

Although MSCs appeared to attach and grow on all samples surface, yet they were found more spreading with extended in multiple directions of filopodium and the growth is accelerated on HA coated samples compared to untreated sample (without HA) as illustrated in Figures 4.7 (c) to (h). This finding suggesting good cell viability on all HA coated samples.

FESEM micrographs in Figures 4.7 (c) and (d) represent the MSCs morphologies on the HA untreated sample (without oxide interlayer). The results indicates that the cells appeared to show less extended of filopodium even after 14 days of incubation. While, Figure 4.7 (e) demonstrates that MSCs were spread out more actively even at day 7. After day 14 (Figure 4.7 (f)), the HA850 sample surface were completely covered with MSCs cells and exhibit greater extensions of filopodium which is looks like a fibers attached to the HA coating surface. This phenomenon shows that an active cell migration on the HA850 sample surface. The multiple microvilli of MSCs cells were also observed until the deepest layers of HA coating as shown in circle area X (Figure 4.7 (f)), which indicating that the sample has good biocompatibility.

Even though, the cells were spread out actively and attached to the HA1050 sample, but after day 14 the breakage of filopodium in MSCs was observed as shown in circle area Y (refer Figure 4.7 (h)). This showed that the attachment of filopodium is not as good as HA850 samples. Comparing to all sample conditions, it is found that the best results were obtained for HA coating sample with oxide interlayer produce at temperature 850°C (HA850).

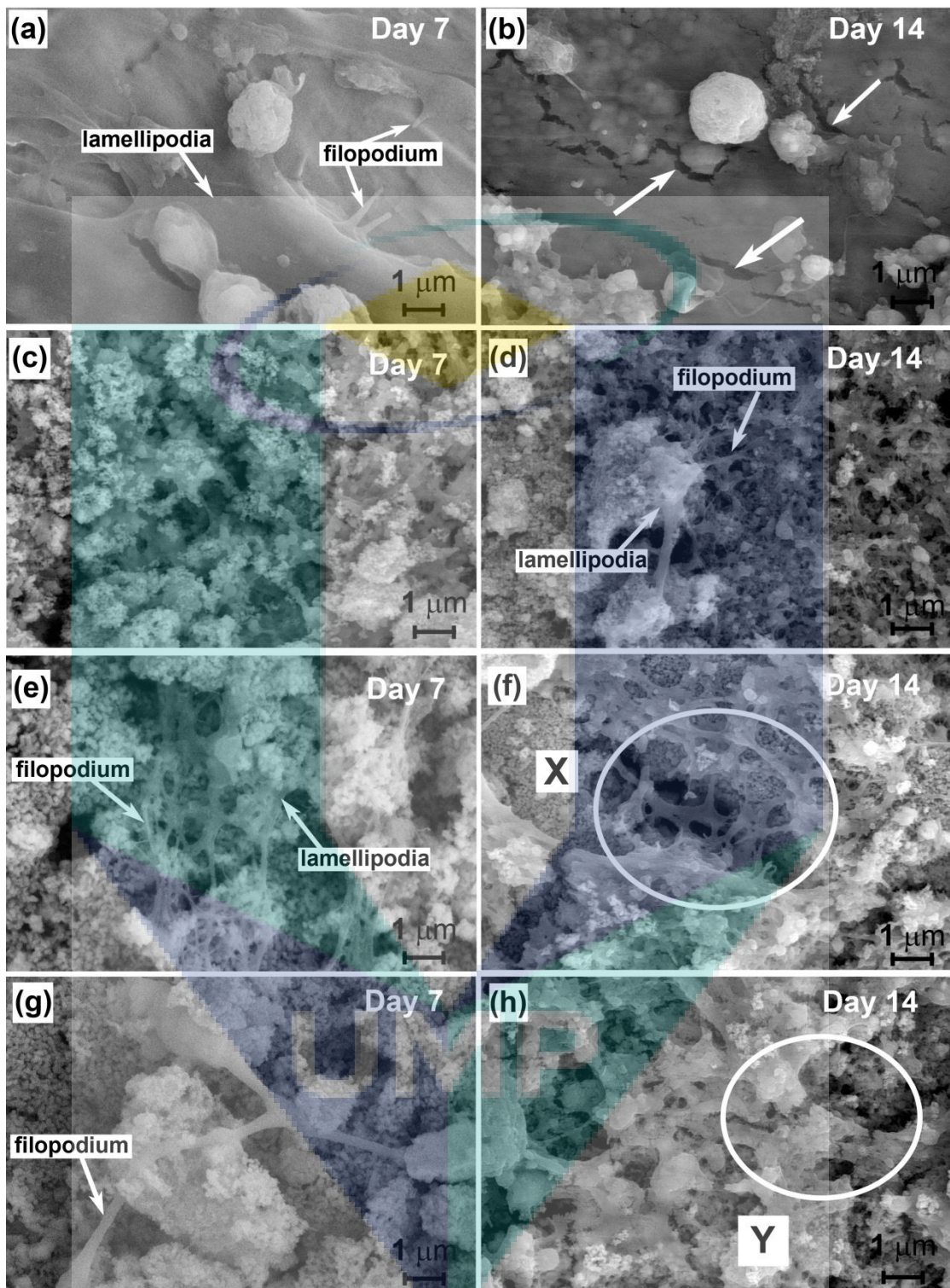


Figure 4.7 FESEM images of MSCs on (a and b) untreated Co-Cr-Mo alloy, (c and d) HAuntreated, (e and f) HA850 and (g and h) HA1050.

CHAPTER 5

CONCLUSIONS AND RECOMMENDATIONS

5.1 Conclusions

The research works done has demonstrated successful results as coating adhesion of HA coating is remarkably improved. The incorporation of oxide interlayer prior to HA coating on this material also has proved greater in cell attachment and has enhances cell proliferation compared with HA coated on untreated sample. Through this research, it is possible to obtain homogeneous crack-free coating, densely packed and uniform coating thickness of HA via sol-gel dip coating technique by modifying metal surface as well as manipulating the HA slurry. The conclusions from this research can be summarized as the following:

- i. The thickness and surface roughness of oxide interlayer highly influenced by thermal oxidation temperature. It is noted that when thermal oxidation temperature increased, the thickness of oxide interlayer is also increased. However, at extremely high temperature (1250°C) used, oxide interlayer was distorted and severe delamination occurred. In terms of surface morphology observation, formation of oxide interlayer at low temperature (850°C) is more uniform and dense when compared to high temperature (1050°C). In the performance of adhesion strength between the oxide interlayer and sample surface, oxide interlayer at 850°C indicated slightly low compared to 1050°C which is 1.25 μm vs. 1.35 μm respectively. The scratch test results obtained from the HA coating on oxidized sample also demonstrate much higher compared to HA coating on untreated sample (1.35N vs. 1N). This result is in line with surface morphology observation, as more uniformity of HA coating,

dense structure and cracks free surface is formed on the oxidized sample than HA on untreated sample. It also can be concluded that rougher surface of oxide interlayer promotes better anchorage of HA particles and provides mechanical interlocking for HA coating to strongly adhered on the sample surface.

- ii. Oxide interlayer introduced on this metal sample also showed positive effects on cells growth as all oxidized samples demonstrated in good attachment of cells and more spreading of filopodium compared to untreated sample and HA on untreated sample.

5.2 Recommendations

Some recommendations regarding this research can be carried out for future works which are:

- (i) For further investigation could be done is by adding binder to HA slurry for example poly ϵ -caprolactone (PCL) as this material approved by the FDA a biodegradable polymer and good biocompatibility properties. The hypothesis results from this future experimental could eliminate the sintering process and at the same time provide better adherence of HA coating on metal implants.
- (ii) The promising results in bioactivity performances achieved via in-vitro test could be extended for further testing such as in-vivo test. Confirmations achieved through in-vivo test will lead this proposed technique for a better understanding of cell responses and generation to new bone growth. Hopefully this approach may help engineers and scientists to come up with better and efficient implants for future usage.

REFERENCES

- [1] Grégory, M., et al., Protection of Cobalt-based Refractory Alloys by Chromium Deposition on Surface. Part II: Behaviour of the Coated Alloys in Oxidation at High Temperature. *Surf. Coat. Technol.*, 2011.
- [2] Blau, P.J., T.M. Brummett, and B.A. Pint, Effects of Prior Surface Damage on High-Temperature Oxidation of Fe-, Ni-, and Co-based Alloys. *Wear*, 2009. 267: p. 380-386.
- [3] McKee, G.K. and J. Watson-Farrar, Replacement of Arthritic Hips by the McKee-Farrar Prosthesis. *J. Bone Joint Surg.*, 1966. 48B(2): p. 245-260.
- [4] Qingliang, W., Z. Lei, and D. Jiandong, Effects of Plasma Nitriding on Microstructure and Tribological Properties of Co-Cr-Mo Alloy Implant Materials. *J. Bionic Eng.*, 2010. 7(4): p. 337-344.
- [5] Santavirta, S., et al., Materials in Total Joint Replacement. *Current Orthopaedics Biomechanics*, 1998. 12: p. 51-57.
- [6] Valero Vidal, C. and A. Igual Muñoz, Effect of Physico-chemical Properties of Simulated Body Fluids on the Electrochemical Behaviour of CoCrMo Alloy. *Electro. Acta*, 2011. 56(24): p. 8239-8248.
- [7] Buscail, H., et al., Oxidation Mechanism of Cobalt Based Alloy at High Temperatures (800-1100°C). *Corr. Eng., Sci. Technol.*, 2012. 47(6): p. 404-410.
- [8] Sameer, R.P. and B.D. Narendra, Calcium Phosphate Coatings for Bio-implant Applications: Materials, Performance Factors and Methodologies. *Mater. Sci. Eng.*, 2009. R 66(1-3): p. 1-70.
- [9] Valero Vidal, C. and A. Igual Muñoz, Effect of Thermal Treatment and Applied Potential on the Electrochemical Behaviour of CoCrMo Biomedical Alloy. *Electrochimica Acta*, 2009. 54(6): p. 1798-1809.
- [10] Türkan, U., O. Öztürk, and A.E. Eroglu, Metal Ion Release from TiN Coated CoCrMo Orthopedic Implant Material. *Surf. Coat. Technol.*, 2006. 200(16-17): p. 5020-5027.
- [11] Hanawa, T., S. Hiromoto, and K. Asami, Characterization of the Surface Oxide Film of a Co-Cr-Mo Alloy After Being Located in Quasi-Biological

- Environments Using XPS. *Applied Surface Science*, 2001. 183(1-2): p. 68-75.
- [12] Cobb, A.G. and T.P. Schmalzreid, The Clinical Significance of Metal Ion Release from Cobalt–Chromium Metal-on-metal Hip Joint Arthroplasty. *Proc. IMechE Part H: J. Engineering in Medicine*, 2005. 220: p. 385-398.
- [13] Duisabeau, L., P. Combrade, and B. Forest, Environmental effect on fretting of metallic materials for orthopaedic implants. *Wear*, 2004. 256(7–8): p. 805-816.
- [14] Geetha, M., D. Durgalakshmi, and R. Asokamani, Biomedical Implants: Corrosion and its Prevention - A Review. *Recent Patents on Corro. Sci.*, 2010. 2: p. 40-54.
- [15] Marcin, M., et al., Release of Metal Ions from Orthodontic Appliances: An In Vitro Study. *Biological Trace Element Res.*, 2012. 146(2): p. 272-280.
- [16] Marjan Bahrami, N., H. Mohd Roshdi, and S. Barkawi, Metallic Biomaterials of Knee and Hip - A Review. *Trends Biomater. Artif. Organs*, 2010. 24: p. 69-82.
- [17] Lu Ning, W. and L. Jing Li, Preparation of Hydroxyapatite Coating on Co-Cr-Mo Implant Using an Effective Electrochemically-assisted Deposition Pretreatment. *Mater. Charac.*, 2011. 62(11): p. 1076-1086.
- [18] Wang, T. and A. Dorner-Reisel, Effect of Substrate Oxidation on Improving the Quality of Hydroxyapatite Coating on CoNiCrMo. *J. Mater. Sci.*, 2004. 39(13): p. 4309-4312.
- [19] DiCarlo, E.F. and P.G. Bullough, The Biologic Responses to Orthopedic Implants and Their Wear Debris. *Clinical Materials*, 1992. 9(3-4): p. 235-260.
- [20] Lewis, A.C., et al., Effect of Synovial Fluid, Phosphate-Buffered Saline Solution and Water on the Dissolution and Corrosion Properties of CoCrMo Alloys as Used in Orthopedic Implants. *J. Biomed. Mater. Res. Part A*, 2005. 73A(4): p. 456-467.
- [21] Keegan, G.M., I.D. Learmonth, and C.P. Case, Orthopaedic Metals and Their Potential Toxicity in the Arthroplasty Patient. *J. Bone Joint Surg*, 2007. 89B: p. 567-563.

- [22] Shuyan, X., et al., RF Plasma Sputtering Deposition of Hydroxyapatite Bioceramics: Synthesis, Performance, and Biocompatibility. *Plasma Process. Polym.*, 2005. 2: p. 373–390.
- [23] Yang, Y., J.L. Ong, and J. Tian, Deposition of Highly Adhesive ZrO₂ Coating on Ti and CoCrMo Implant Materials Using Plasma Spraying. *Biomaterials*, 2003. 24(4): p. 619-627.
- [24] Escobedo Bocardo, J.C., et al., Apatite Formation on Cobalt and Titanium Alloys by a Biomimetic Process. *Adv. Technol. Mater. & Mater. Process.*, 2005. 7(2): p. 141-148.
- [25] Surmenev, R.A., M.A. Surmeneva, and A.A. Ivanova, Significance of calcium phosphate coatings for the enhancement of new bone osteogenesis – A review. *Acta Biomaterialia*, 2014. 10(2): p. 557-579.
- [26] Mudenda, S., et al., Effect of Substrate Patterning on Hydroxyapatite Sol–gel Thin Film Growth. *Thin Solid Films*, 2011. 519(16): p. 5603-5608.
- [27] Dong-Yang, L. and W. Xiao-Xiang, Electrodeposition of Hydroxyapatite Coating on CoNiCrMo Substrate in Dilute Solution. *Surf. Coat. Technol.*, 2010. 204(20): p. 3205-3213.
- [28] Ling, L., et al., Effects of Surface Roughness of Hydroxyapatite on Cell Attachment and Proliferation. *J. Biotechnol. Biomater.*, 2012. 2(6): p. 1-5.
- [29] Bikramjit, B. and K. Mitjan, Overview: Bioceramics and Biocomposites. 1st. ed. *Tribology of Ceramics and Composites*, ed. USA. 2011, USA: John Wiley & Sons, Inc.
- [30] Wang, Y., et al., Osteoblastic Cell Response on Fluoridated Hydroxyapatite Coatings. *Acta Biomater.*, 2007. 3(2): p. 191-197.
- [31] Ergun, C., R.H. Doremus, and W.A. Lanford, Interface Reaction/diffusion in Hydroxylapatite-Coated SS316L and CoCrMo Alloys. *Acta Mater.*, 2004. 52(16): p. 4767-4772.
- [32] Yunzhi, Y., K. Kyo Han, and L.O. Joo, A Review on Calcium Phosphate Coatings Produced Using a Sputtering Process—An Alternative to Plasma Spraying. *Biomaterials.*, 2005. 26(3): p. 327-337.
- [33] Cortes, D.A., et al., Biomimetic Apatite Formation on a CoCrMo Alloy by Using Wollastonite, Bioactive Glass or Hydroxyapatite. *J. Mater. Sci.*, 2005. 40: p. 3509 – 3515.

- [34] Cortés-Hernández, D.A., et al., Biomimetic Bonelike Apatite Coating on Cobalt Based Alloys. *Mater. Sci. Forum*, 2003. 442: p. 61-66.
- [35] Escobedo, J.C., et al., Hydroxyapatite Coating on a Cobalt Base Alloy by Investment Casting. *Scripta Mater.*, 2006. 54: p. 1611–1615.
- [36] Leon, B. and J.A. Jansen, *Thin Calcium Phosphate Coatings for Medical Implants*. 2nd. ed. 2009, New York: Springer.
- [37] Brinker, C.J., et al., *Fundamentals of Sol-gel Dip Coating*. *Thin Solid Films*, 1991. 201(1): p. 97-108.
- [38] Sunho, O., et al., Surface Characterization and Dissolution Study of Biodegradable Calcium Metaphosphate Coated by Sol-gel Method. *J. Sol-Gel Sci. Technol.*, 2010. 53(3): p. 627-633.
- [39] Liu, X., P.K. Chu, and C. Ding, *Surface Modification of Titanium, Titanium Alloys and Related Materials for Biomedical Applications*. *Mater. Sci. Eng.: R: Reports*, 2004. 47(3-4): p. 49-121.
- [40] Brinker, C.J., et al., Review of Sol-gel Thin Film Formation. *J. Non-Crystalline Solids*, 1992. 147–148: p. 424-436.
- [41] Purna, C.R., et al., Titania/hydroxyapatite Bi-layer Coating on Ti Metal by Electrophoretic Deposition: Characterization and Corrosion Studies. *Ceram. Int.*, 2012. 38(4): p. 3209-3216.
- [42] Jian, W., et al., Fluoridated Hydroxyapatite Coatings on Titanium Obtained by Electrochemical Deposition. *Acta Biomater.*, 2009. 5(5): p. 1798-1807.
- [43] Nadim, J.H., et al., Evaluation of Metallic and Polymeric Biomaterial Surface Energy and Surface Roughness Characteristics for Directed Cell Adhesion. *Tissue Engineering*, 2001. 7: p. 55-72.
- [44] Valero Vidal, C. and A. Igual Muñoz, Effect of Physico-chemical Properties of Simulated Body Fluids on the Electrochemical Behaviour of CoCrMo Alloy. *Electro. Acta*, 2011. 56(24): p. 8239-8248.
- [45] Yuling Yang, et al., Osteoblast Interaction With Laser Cladded HA and SiO₂-HA Coatings on Ti-6Al-4V. *Mater. Sc. Eng. C*, 2011. 31: p. 1643-1652.

APPENDIX A

Gantt Charts and Milestone of Research Activities

	Research Activities	First Year												Second Year											
		1	2	3	4	5	6	7	8	9	10	11	12	1	2	3	4	5	6	7	8	9	10	11	12
1	Literature review	■	■	■	■	■	■	■	■	■	■	■	■	■	■	■	■	■	■	■	■	■	■	■	■
2	Sample Preparation			■	■	■	■	■	■	■	■	■	■												
3	HA Slurry Preparation & Coating Deposition						■	■	■	■	■	■	■												
4	Biocompatibility Test									■	■	■	■												
5	Analysis results																	■	■	■	■	■	■	■	■
6	Publication and report writing																								■

	Milestones	First Year												Second Year											
		1	2	3	4	5	6	7	8	9	10	11	12	1	2	3	4	5	6	7	8	9	10	11	12
1	To complete HA slurry preparation & coating deposition						■																		
2	To complete characterisation of HA coated samples										■														
3	To complete adhesion strength test																■								
4	To complete biocompatibility test																					■			
5	To complete preparing technical publications & report closure																								■

UMP

APPENDIX B

Pattern : 00-038-1479		Radiation = 1.540600		Quality : High		
<p>Cr₂O₃</p> <p>Chromium Oxide Also called: chrome green, green cinnabar, Eskolaite, syn</p>		2 θ	<i>i</i>	<i>h</i>	<i>k</i>	<i>l</i>
		24.494	73	0	1	2
		33.597	100	1	0	4
		36.196	93	1	1	0
		39.749	7	0	0	6
		41.480	35	1	1	3
		44.194	6	2	0	2
		50.220	38	0	2	4
		54.852	87	1	1	6
		57.111	1	2	1	1
		58.397	7	1	2	2
		63.449	28	2	1	4
		65.106	39	3	0	0
		72.944	14	1	0	10
		73.329	6	1	1	9
		76.851	9	2	2	0
		79.056	6	3	0	6
		80.200	1	2	2	3
		82.092	4	3	1	2
		84.239	7	0	2	10
		85.682	2	0	0	12
		86.539	7	1	3	4
		90.202	13	2	2	6
		93.193	1	0	4	2
		95.328	9	2	1	10
		96.734	1	1	1	12
		97.591	2	4	0	4
		104.385	1	2	3	2
		106.995	1	2	2	9
		108.985	6	3	2	4
		110.588	5	4	1	0
		114.145	1	4	1	3
		118.608	7	1	3	10
		120.267	3	3	0	12
		121.081	1	2	0	14
		125.624	10	4	1	6
		132.174	3	4	0	10
		134.164	1	2	2	12
		135.174	6	1	2	14
		135.363	3	0	5	4
		137.504	4	3	3	0
		149.845	5	3	2	10
<p>Lattice : Rhombohedral</p> <p>S.G. : R-3c (167)</p> <p>a = 4.95876</p> <p>c = 13.59420</p> <p>Z = 6</p>		<p>Mol. weight = 151.99</p> <p>Volume [CD] = 289.49</p> <p>Dx = 5.231</p>				
<p>Additional Patterns: To replace 00-006-0504, Swanson et al. (3). See PDF 01-084-1616, 01-082-1465 and 01-084-0312. Color: Dark grayish yellow-green. Powder Data: Further literature citations may be found in reference 3. Sample Preparation: Chromium nitrate hydrate, "Cr (NO₃)₃ · 9 H₂O", was heated to 500 C for 4 hours then annealed at 1200 C for 1 day in a chromium crucible. Structures: The structure of chromium oxide was determined by Wretblad (1) and later on was redetermined by Saalfeld (2). Temperature of Data Collection: The mean temperature of data collection was 299.1 K. Unit Cell Data Source: Powder Diffraction. Data collection flag: Ambient.</p>						
<p>McMurdie, H., Morris, M., Evans, E., Paretzkin, B., Wong-Ng, W., Zhang, Y., Powder Diffraction, volume 2, page 45 (1987)</p> <p>CAS Number: 1308-38-9</p>						
<p>Radiation : CuKα1</p> <p>Lambda : 1.54060</p> <p>SS/FOM : F30= 76(0.0099,42)</p>		<p>Filter : Monochromator crystal</p> <p>d-sp : Diffractometer</p>				

APPENDIX C

Pattern : 00-033-0892		Radiation = 1.540600		Quality : Blank		
$Mn_{1.5}Cr_{1.5}O_4$ Manganese Chromium Oxide		2th 18.164 29.910 35.236 36.837 42.824 53.112 56.593 62.121 73.462 74.473 75.445	i 25 50 100 6 20 10 30 45 6 2 2	h 1 2 3 2 4 4 5 4 5 6 2	k 1 2 1 2 0 2 1 4 3 2	l 1 0 1 2 0 2 1 0 3 2
Lattice : Face-centered cubic S.G. : Fd-3m (227) a = 8.45500		Mol. weight = 224.40 Volume [CD] = 604.42				
General Comments: Semiconducting between -193 C and +300 C. Color: Brownish black. Sample Preparation: Produced by reaction: "6 Mn Cr O3" = "4 Mn1.5 Cr1.5 O4" + "O2" between 690 ° and 1150 C or by heating "Cr2 O3" + "Mn2 O3" at 1000 C for 20 hours. Data collection flag: Ambient.						
Chamberland, B. et al., Inorg. Chem., volume 16, page 44 (1977)						
Radiation : CuK α Lambda : 1.54180 SS/FOM : F10= 10(0.0692,14)		Filter : d-sp : Diffractometer				

APPENDIX D

Pattern : 01-071-7109		Radiation = 1.540600		Quality : Indexed			
(Co _{0.8} Cr _{0.2})		2th		<i>i</i>	<i>h</i>	<i>k</i>	<i>l</i>
Cobalt Chromium		41.337	270	1	0	0	0
		44.577	275	0	0	0	2
		47.241	999	1	0	0	1
		62.410	111	1	0	0	2
		75.374	98	1	1	0	0
		84.058	95	1	0	0	3
		89.809	12	2	0	0	0
		92.017	89	1	1	1	2
		93.933	62	2	0	0	1
		98.672	12	0	0	0	4
		106.520	14	2	0	0	2
		113.574	12	1	0	0	4
		130.089	30	2	0	0	3
		138.087	9	2	1	0	0
		144.694	56	2	1	1	1
Lattice : Hexagonal		Mol. weight = 57.55					
S.G. : P63/mmc (194)		Volume [CD] = 22.34					
a = 2.52000	Z = 2	Dx = 8.555					
c = 4.06200		I/Cor = 6.56					
<p>ANX: N. Formula from original source: (Co0.8 Cr0.2). ICSD Collection Code: 102317. Test from ICSD: At least one temperature factor missing in the paper. Minor Warning: No R factors reported/abstracted. No e.s.d reported/abstracted on the cell dimension. Minor test comments from ICSD exist. Unit Cell Data Source: Powder Diffraction. Data collection flag: Ambient.</p>							
<p>Calculated from ICSD using POWD-12++ Jongebreur, R., van Engen, P.G., Buschow, K.H.J., J. Magn. Magn. Mater., volume 38, page 1 (1983)</p>							
Radiation : CuKα1		Filter :					
Lambda : 1.54060		d-sp : Calculated spacings					
SS/FOM : F15=1000(0.0000,15)							

APPENDIX E**Publications**

1. R. I. M. Asri, W. S. W. Harun, **M. A. Hassan**, S. A. C. Ghani, Z. Buyong (2016), “A review of hydroxyapatite-based coating techniques: Sol–gel and electrochemical depositions on biocompatible metals”, *Journal of the Mechanical Behavior of Biomedical Materials*, 57 (2016) 95 – 108. (Published)
2. **H. Mas Ayu**, S. Izman, R. Daud, G. Krishnamurithy, A. Shah , S. H. Tomadi and M. S. Salwani (2017), “Surface Modification on CoCrMo Alloy to Improve the Adhesion Strength of Hydroxyapatite Coating”, *Procedia Engineering*, 184 (2017) 399 – 408. (Published)
3. **H. Mas Ayu**, S. Izman, R. Daud, , A. Shah, Mohd Faiz Mohd Yusoff, G. Krishnamurithy, T. Kamarul (2017), “In-Vitro Biocompatibility Study of Hydroxyapatite Coated on Co-Cr-Mo With Oxide Interlayer”, *Jurnal Teknologi*. (Waiting to be published).
4. **H. Mas Ayu**, R. Daud, A. Shah, M. Y. Mohd Faiz, H. M. Hazwan, M. S. Salwani, S. H. Tomadi, M. S. Reza (2017), “Thermal Oxidation Process Improved Corrosion in Cobalt Chromium Molybdenum Alloys”, *International Journal of Advanced and Applied Sciences*. (Waiting to be published).